A calibration procedure for the assessment of work hardening part I: Effects of the microstructure and load type

J.P. Goulmy, E. Rouhaud, P. Kanoute, L. Toualbi, S. Kruch, V. Boyer, J. Badreddine, D. Retraint

PII: S1044-5803(21)00197-2

DOI: https://doi.org/10.1016/j.matchar.2021.111067

Reference: MTL 111067

To appear in: *Materials Characterization*

Received date: 26 November 2020

Revised date: 24 March 2021

Accepted date: 25 March 2021

Please cite this article as: J.P. Goulmy, E. Rouhaud, P. Kanoute, et al., A calibration procedure for the assessment of work hardening part I: Effects of the microstructure and load type, *Materials Characterization* (2021), https://doi.org/10.1016/j.matchar.2021.111067

A calibration procedure for the assessment of work hardening Part I: effects of the microstructure and load type.

J.P. Goulmy[1], E. Rouhaud[2], P. Kanoute[3], L. Toualbi[3], S. Kruch[3], V. Boyer[2], J. Badreddine[4], D. Retraint[2]

[1]Arts et Metiers Institute of Technology, MSMP, HESAM Université, F-13617 Aix-en-Provence, France

[2]Laboratoire des Systèmes Mécaniques et d'Ingénierie Simultanée (LASMIS), Institut Charles Delaunay (ICD), Université de Technologie de Troyes (UTT), 10000 Troyes, France

[3]Onera - The French Aerospace Lab, Département Matériaux et Structures, F-92322 Châtillon, France

[4]Safran Tech, Materials & Processes department, Rue des Jeunes Bois, 78772 Magny-Les-Hameaux, France

Corresponding author : jean-patrick.*goulmy@ensam.eu* (J.P. Goulmy)
(+33) 4 42 93 82 23

Abstract

This paper presents a methodology to define and quantify the level of work hardening locally in a material. The methodology is proposed after a thorough experimental study based on three complementary experimental techniques for microstructural characterizations: microhardness, X-ray diffraction (XRD) and Electron Backscatter Diffraction (EBSD) applied on Inconel 718 samples. In our analysis, several loading histories including single tension, single compression, high strain rates and low cycle fatigue have been investigated. The effects of the microstructure have been further investigated by modifying the size of the grains and the size of the strengthening precipitates. Experimental tests have also been simulated to choose a model variable able to represent work hardening. A reciprocal link between work hardening and experimental characterizations has then been established. Correlation curves have been proposed that enable to quantify the level of work hardening from the knowledge of the experimental data. Accuracy and complementarity of the three experimental approaches are discussed as well as the impact of the microstructure of the material on the measured quantities.

Keywords: Inconel 718; work hardening; calibration; XRD; EBSD

Introduction

In order to accurately predict fatigue behavior and crack initiation in metallic components, it is fundamental to possess a realistic picture of the initial state of the material. The processes used to manufacture the parts have indeed introduced plastic deformation, work hardening and also may have changed the local microstructure of the metal. The strain incompatibilities hence generated, have further induced a residual stress field. Residual stresses are not the only quantity that influences fatigue life [1]–[9], another relevant quantity being the level of work hardening accumulated in the material. Indeed, for the same amount of residual stress observed locally, the level of work hardening may vary. It is further observed that the evolution of the mechanical fields during thermo-mechanical cyclic loadings, the evolution of the stress state, in particular, is strongly influenced by this initial work hardening level as detailed by Prevey [1]. Thus, the initial state to be considered has to be specified, not only with the knowledge of the residual stress field, but also with the knowledge of the consequences of the load history of the material during manufacturing. In the end, both the residual stress field and work hardening, have to be taken into account to define an initial state that is far from being the "neutral configuration" that one would wish to consider to evaluate fatigue.

The term "hardening" has several (related) meanings depending on the communities. It is a term used to refer to the increase in yield stress to refer to model types and variables (like for example isotropic or kinematic hardening…), or to describe the level of disorder in a local microstructure. Further, work hardening and its effects are not only a function of the amplitude of the applied load, but seem to be influenced by other factors like, for example, the imposed strain rate [10]. This quantity is also strongly impacted by the local microstructure of the material that may further present a gradient in grain size, precipitate size, and that may also evolve in service [1], [11], [12].

The recent improvements of experimental techniques such as X-ray diffraction (XRD) and electron backscatter diffraction (EBSD) have rendered possible numerous studies correlating work hardening to other experimental data. Several authors have proposed procedures to quantify work hardening

[13], [14], [10], [15]–[18]. These studies present a significant complementarity between experimental techniques like XRD, EBSD and microhardness [13]–[16], [19], [20]. In particular, Soady et al. compare these three techniques and propose a conversion between plastic strain and work hardening [16].

However, open questions remain concerning the level of work hardening reached in the material as a function of the initial microstructure and during the life cycles of a component. It is particularly interesting to investigate the influence of the local microstructure in regard to the temperature and the strain rates endured by the material.

The purpose of this paper is thus to propose a methodology to define and quantify the level of work hardening locally in a material, taking into account the influence of the type of loading, the temperature, the strain rate and the microstructure. The methodology is proposed after a thorough experimental study based on three different experimental techniques: microhardness, XRD and EBSD applied on Inconel 718 samples. This material is widely used for aeronautical applications such as high-pressure turbine disks. The knowledge on the mechanical state is of primary importance for fatigue life estimation. An original method, allowing defining work hardening with respect to a variable of a behaviour law, is then presented. For this, numerical simulations of experimental tests are performed. A reciprocal link between this variable and the experimental characterizations is then established. The range of applicability of the procedure along with the influence of the experimental parameters taken into account are finally discussed.

1 Methodology

It is not possible to directly measure work hardening experimentally. Indeed, this term characterizes a set of physical quantities and mechanical phenomena related to the level of disorder reached in the microstructure of the material. In order to build a calibration procedure able to evaluate work hardening, four steps have been followed as described in the next paragraphs:

First, a large set of mechanical tests has been performed to evaluate the influence of the following parameters:

- The type of loading:

  Classical uniaxial tensile tests have been performed along with cyclic tests and compressive tests. The objective was to investigate different types of loadings at various levels of plastic deformation. The compressive tests enabled to reach higher strain rates. Fatigue tests have also been performed to evaluate the influence of cyclic loading.

- The temperature:

  Two temperatures have been investigated the ambient temperature (20°C) and 550°C. The latter has been chosen to represent the life cycle conditions of the material and to enable comparison with experimental data available in the literature [21].

- The strain rate:

  A quasi-static strain rate of 10^{-3} s^{-1} has been chosen for tensile and compressive tests. The cyclic tests have then been performed with the same 10^{-3} s^{-1} for comparison. Compressive tests with higher rates have been finally completed to consider conditions representative of what could be encountered during manufacturing processes.

- The microstructure:

  Three microstructures have been investigated to evaluate the influence of grain and precipitate size on work hardening and the sensibility of the calibration procedure.

Table 1 presents an exhaustive description of the experimental campaign completed in this study. To facilitate the interpretation of the data, colored symbols have been associated to each test condition; this graphic code is applied throughout this article. Section 2.2 details the experimental conditions of the tests.

The second step consists in identifying experimental quantities able to represent work hardening in the material. Three experimental methods: microhardness, XRD and EBSD, have been applied to the samples for characterization. Several quantities have been measured that are related to the level of defects in the microstructure. These quantities are the microhardness, the peak width of the X-ray diffracted signal (FWHM, full width at half maximum), the kernel average misorientation (KAM) issued from EBSD measurements. Both the intensity of each quantity and its evolution with the load have been monitored. These three experimental quantities have been chosen because they give a complementary evaluation of the state of the material. The experimental conditions for these three techniques are detailed in section 2.3 along with their definitions and the justification for this choice. Table 1 presents the type of experimental measurements performed on each sample.

We have next identified a model variable able to quantify work hardening. The third step consists thus in modelling each of the mechanical tests performed on the different samples, as described above in step 1. An elasto-plastic model has been chosen to describe the material and several variables have been identified as potential candidate to represent work hardening in the material. The numerical results obtained after computation have been correlated with the experimental data obtained in step 2. Then, the model variable that best correlates the experimental results has been selected to represent work hardening in the material. This is presented in section 3.

Finally, a correlation between each experimental quantity and the variable chosen to model work hardening has been established. A set of functions has been built, fitting the data (see section 4). This set of functions can then be used to correlate experimental measurements in a given material to the variable chosen to represent work hardening.

In the end, we dispose of a calibration method to evaluate work hardening locally in the chosen material.

Table 1. Test conditions for calibration specifying the microstructure, the applied load, the range of plastic deformation that has been reached, the temperature, the strain rate, the experimental techniques used on each sample and the graphic code used in this article. A total of 30 tests has been performed.

Microstructure	Test condition	Quantity	Range of plastic strain	Temperature (°C)	Strain rate (s^{-1})	Technical analysis	Symbol
Direct Aged	Tensile	5	[0.05-0.15]	20	10^{-3}	XRD, EBSD, Microhardness	■
	Tensile	2	[0.01-0.015]	550	[illegible]	XRD	▲
	Compressive	3	[0.3-0.4]	20	[illegible]	XRD, EBSD	●
	Compressive	5	[0.1-0.3]	20	[illegible] 10^{-3}	XRD	▬
	Cyclic	1	[0.0008, 0.009]	20	10^{-3}	XRD, EBSD	◆
	Cyclic	1	[0.0006]	55[illegible]	10^{-3}	XRD	★
Coarse grain	Tensile	5	[0.05-0.15]	[illegible]0	10^{-3}	XRD, EBSD, Microhardness	■
	Compressive	3	[illegible]3-0.4[illegible]	20	10^{-3}	XRD, EBSD	●
Coarse grain and coarse strengthening precipitates	Tensile	5	[illegible]05-0.15]	20	10^{-3}	XRD, EBSD, Microhardness	■

2 Experimental campaign

2.1 Inconel 718

All the samples have been extracted from an Inconel 718 Direct Aged (*DA*) turbine disk, the composition of which is given in Table 2. Three microstructures of this alloy have been investigated. The first microstructure (named *Direct aged microstructure* in the following) is the *reference* microstructure, obtained directly after forging and corresponding to the "as-received" material. The two other microstructures correspond to the reference microstructure further modified by applying

either one of the following heat treatments:

- The second microstructure is a *coarse grain microstructure* obtained through an annealing at 1040 °C during 30 minutes (temperature above the δ phase solvus), followed by a δ phase precipitation treatment at 955 °C for one hour, next followed, by the conventional $\gamma'+\gamma''$ precipitation treatment, performed at 720 °C during 8 hours, itself followed by a cooling at 50 °C/h and finally, an aging at 620 °C for 8 hours.
- The third microstructure includes *coarse grain and coarse strengthening precipitates* obtained with the same heat treatment sequence as the second one, except for the final precipitation treatment of the γ' and γ'' phases: an overaging at 750 °C for 50 hours is applied instead, in order to modify the size of the precipitates.

Note that a color code is used to reference the three microstructures as presented in Table 3; this code will be used throughout this article.

The characterization of the microstructures has been carried out by scanning electron microscopy observations and backscattered electron analyses (see Table 3). The mean grain size and the mean size of the strengthening precipitates of these three microstructures are further detailed in Table 3. A grain size of about 5 µm is obtained for the direct aged microstructure while grains of about 35 µm are obtained for the two other microstructures. The strengthening precipitates have similar sizes in the direct aged microstructure and the *coarse grain* microstructure (10 to 20 nm), whereas the size of the strengthening precipitates is ranging from 100 to 200 nm for the *coarse grain and coarse strengthening precipitate* microstructure. In addition to the strengthening precipitates, Inconel 718 is composed of a δ phase, a stable version of the γ'' phase that controls the grain size. Nitrides and carbides are also present and have a size in the order of 10 to 15 µm. Note that heat treatments performed to modify the microstructure do not influence the presence of the nitrides and carbides. The delta phase, which is dissolved during the annealing at 1040°C, is re-precipitated with a size and a volume fraction which is similar to the initial ones.

Thus, comparing the reference microstructure (direct aged microstructure) and the *coarse grain* microstructure enables to evaluate the influence of the grain size. The comparison of the *coarse grain* microstructure with the *coarse grain and coarse strengthening precipitate* microstructure enables to evaluate the influence of the size of the hardening precipitates.

Table 2. Composition of the Inconel 718 *DA* Alloy provided by the manufacturer (Wt%).

Ni	Fe	Cr	Mo	Al	Ti	Nb	Si	C
54.18	17.31	17.97	2.97	0.56	1	5.3	0.1	0.023

Table 3. Scanning electron microscopy observations and mean grain size and size of the strengthening precipitates for the microstructures investigated. Throughout this article, the reference microstructure is always referenced in blue, the *coarse grain* microstructure in red and *coarse grain* and *coarse strengthening precipitate* microstructure in orange.

	Direct Aged microstructure	**Coarse grain microstructure**	**Coarse grain and coarse strengthening precipitate microstructure**
Grains	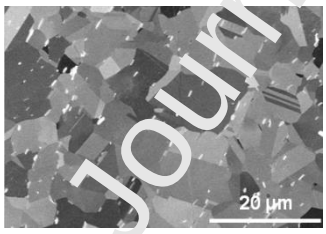	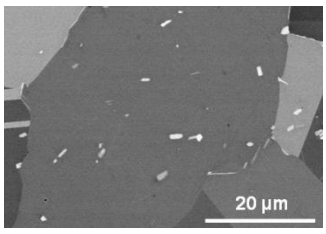	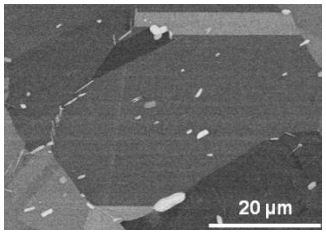
Strengthening precipitates	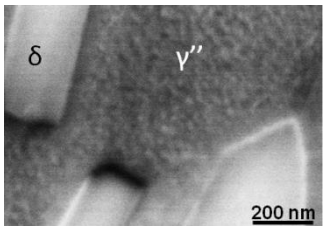	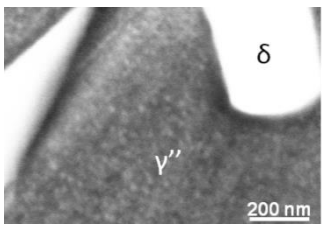	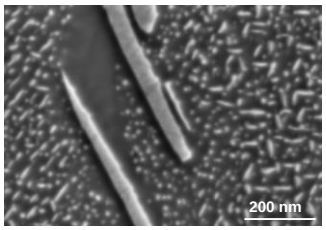
Mean grain size (µm)	4.2	34.7	36.8
Strengthenin	~ 10 - 20	~ 10 - 20	~ 100 – 200

g precipitates size (nm)			

2.2 Mechanical tests

The samples have been submitted to different types of loading able to generate plastic deformation. During the tests, the mechanical fields are controlled to remain homogenous throughout the gauge length of each sample. Precautions have thus been taken to insure that the samples are free of residual stresses at the end of the test. Stress and strain levels were monitored as a function of time throughout the tests. The experimental settings, specific to each applied load, are detailed below.

The uniaxial tensile tests and fatigue tests have been performed on a MTS machine with a force cell of 10 kN, a controlled strain rate of 10^{-3} s^{-1} and an extensometer to determine the strain. The samples were cylindrical with a diameter of 4.37 mm. For the tensile tests, five levels of plastic deformation have been investigated; Table 4 presents the values that has been reached in each sample. Figure 1 presents the stress strain curves for each test. The cyclic tests were strain controlled and performed with the same rate as the tensile tests for two levels of plastic deformation as specified in Table 1 and for a strain ratio equal to zero.

The quasi-static compressive tests have been performed on an Instron 5584 machine with a force cell of 150 kN. The samples were cylindrical specimens with a diameter of 6 mm and a height of 6 mm. The strain rate was controlled at 10^{-3} s^{-1}. The results are presented in Table 4.

The high rate compressive tests have been performed on several Hopkinson type devices in the facilities of CRED (Centre de Ressources en Essais Dynamiques) [22]. A rapid camera could monitor the tests to evaluate the global compressive displacement of the cylinder as a function of time with a precision of 0.05 mm. Several strain rates have been tested between 1100 s^{-1} and 4100 s^{-1}. The spanned interval of plastic deformation is ranging from 0.1 to 0.3.

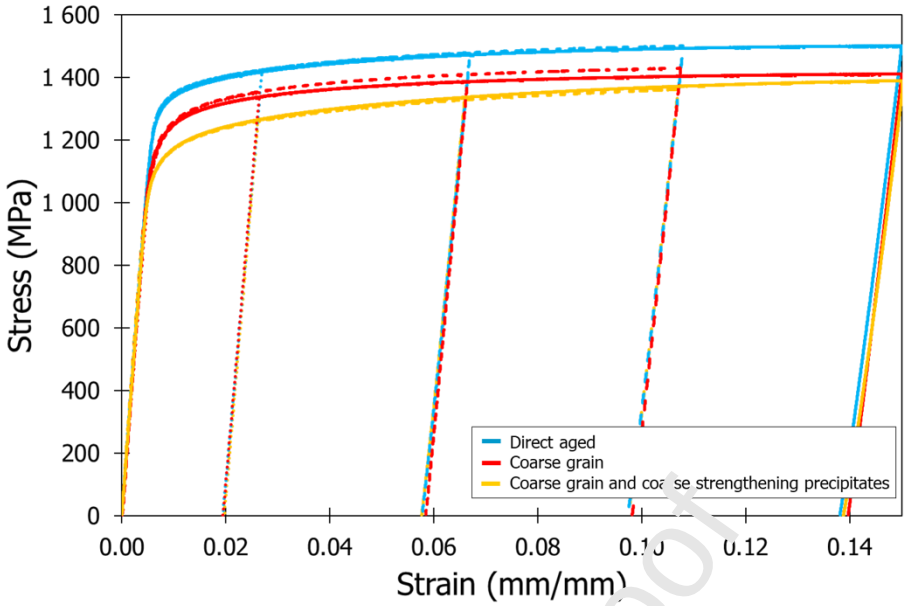

Figure 1. Experimental stress strain curves of the tensile tests for the three microstructures and for the various end-levels of plastic deformation.

Table 4. Values of the plastic deformation reached in the samples submitted to tensile and compressive tests as illustrated in Figure 1 and for the three microstructures.

		Plastic deformation		
Test number	Test condition	Direct aged	Coarse grain	Coarse grain and coarse strengthening precipitate
1	Tensile 10^{-3} s^{-1}	0.019	0.019	0.020
2		0.058	0.059	0.058
3		0.097	0.098	0.098
4		0.138	0.114	0.139
5	Compressive 10^{-3} s^{-1}	0.323	0.377	-
6		0.326	0.397	-
7		0.38	0.387	-

2.3 Material characterization

After deformation, the different samples have been characterized using microhardness technique,

XRD and EBSD. The experimental conditions for these measurements are presented in the following sections.

2.3.1 Microhardness measurement technique

This technique, relatively easy to implement, is sensitive to several parameters and in particular to the microstructure, the work hardening level and the residual stresses in the material. Microhardness has long been used to evaluate the yield strength of polycrystalline materials [23]–[25]. The link between microhardness and yield strength could be explained by strain hardening and the associated increase in dislocation density that raises the resistance to plastic strain

The samples have been extracted from the test specimens by cutting; it has been verified that they were free of residual stresses. All cross sections have been prepared by mechanical polishing up to 1 µm with diamond paste followed by colloidal silica in order to achieve mirror polished flat surfaces free from damage.

The tests have been performed on a BUEHLER device using a Vickers indenter (pyramidal shape) with a load of 100 grams for 10 seconds. The observation of the indents showed that their diagonal was 20 µm on average. This load was chosen to obtain indentation sizes allowing the calibration method to be used to evaluate microhardness gradients at depth. To evaluate the hardness of a given sample, 10 indents have been performed on its surface and averaged. The state of the material is thus evaluated on a volume of approximately 1300 μm^3. This volume includes more than one grain for the *DA* microstructure and less than one for the *coarse grain* microstructure and *coarse grain and coarse strengthening precipitate* microstructure. The results are presented in section 4.1.

2.3.2 X-ray Diffraction

X-ray diffraction techniques allow an indirect evaluation of work hardening with the determination of the peak width of the diffracted signal. Several parameters can lead to a variation in this width, coming from instrumental and experimental contributions. The experimental contribution depends

in particular on the size of the grains and substructures, the work hardening of the material and the different phases involved [26]. Because the analyzed volume is usually large compared to the size of the grains, the values of the full width at half maximum of the peaks (FWHM) display information on both intergranular and intragranular work hardening.

A Seifert PTS diffractometer with a Co-Kα tube radiation ($\lambda_{Co\text{-}K\alpha}$= 1.79 Å) has been used to perform the measurements on the 311 diffraction peak at a 2θ angle of about 111° (accelerating voltage: 20 kV, nominal current: 4 mA). The sample preparation is identical to the one performed for microhardness measurements. With these conditions, the X-ray penetration depth is estimated to be between 2 and 4 µm and the size of the analyzed volume is a few millimeters wide.

The X-ray data have been processed with classical methods [26]. The diffraction peaks have been modelled by a pseudo-Voigt function, and the FWHM of this function has been evaluated. The classical $\sin^2\psi$ method combined with material removal by electrochemical etching has been used to determine the residual stress profile in each studied specimen (results not presented in this paper) as well as the in-depth line broadening profile defined by the FWHM. For each depth, an average taking into account eleven ψ angles have been used to estimate the FWHM parameter. The results are presented in section 4.2.

2.3.3 Electron BackScatter Diffraction

This technology is used to identify crystallographic phases, grain size and crystallographic local orientations. Several authors have highlighted a relationship between local misorientations determined by EBSD and the accumulation of geometrically necessary dislocations [27]. We have chosen to evaluate a kernel average misorientation (KAM) parameter from the EBSD measurements. The KAM parameter represents the average value of the misorientation between the considered pixel and its *N* first neighbors, i.e. the *N*th first adjacent pixels (Figure 2). A correlation between KAM and plastic strain has been found in several papers for nickel base alloys and steel materials [14], [18],

[28].

The volume analyzed by EBSD is of a few micrometers in depth for surfaces up to hundreds of square micrometers. This is much smaller than the volume analyzed with X-ray diffraction. This technique gives thus a very local information on the material, and, depending on the device, the resolution can be as fine as hundreds of nanometers. It gives access to a partial quantification of the dislocation density, since only the geometrically necessary dislocations are detected [27], [29]. These dislocations are characteristic of a non-uniform plastic deformation of the material, preferentially localized on the grain boundaries [14], [30]. As the geometrically necessary dislocations density is mainly sensitive to activities close to the grain boundaries, the KAM value measured by EBSD are sensitive to the microstructure.

The sample preparation was identical to the one performed for X-ray diffraction and microhardness measurements followed by a final ion polishing to eliminate any strain hardening induced by previous mechanical polishing steps.

The data has been collected using a NORDIF CD camera operating at 30 fps coupled to a MERLIN Scanning Electron Microscope operating at an accelerating voltage of 20 kV and a nominal current of 40 nA. The square pattern size corresponds to 1024 x 512 pixels for 512 x 256 μm^2 fields, with a step size of 0.5 µm. Under these conditions:

- 10 pixels are dedicated to each grain on average, for the finest microstructure (remember that the finest microstructure has a mean grain size of 5 µm),
- 20 grains are investigated in the width of the EBSD window on average for the overall field for the *coarse* microstructure (remember that the *coarse* microstructure has a mean grain size of 40 µm).

The chosen resolution is thus sufficiently refined to enable accurate measurements and analyses.

Further, the influence of the parameter *N* in the KAM computation has been evaluated. The value of *N* has been varied and the results show that there is no influence of this parameter in the present

study. Its value has thus been set to one. The KAM values displayed in sections 3 and 4 correspond to the mean values of the observed fields. The results are presented in section 4.3.

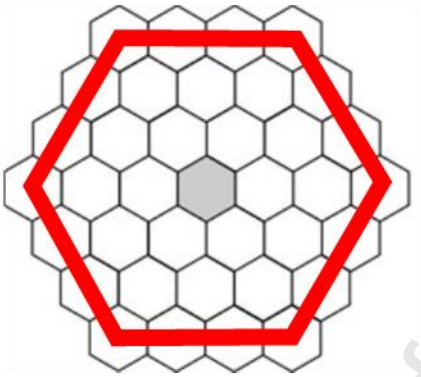

Figure 2. Evaluation of the KAM parameter: misorientation between the considered pixel, at the center, with respect to its N first neighbors (N = 3 for the neighbors in red).

3 Choice of a model variable to evaluate hardening

The expression *work hardening* describes a complex reality associated to the set of physical phenomena observed in metals when submitted to irreversible deformations. To establish a calibration procedure, it is necessary to select a model quantity that is able to capture enough of these phenomena to be able to characterize a work hardening state. The objective of this section is thus to explore different classical variables defined in constitutive models for plasticity in order to test whether they could be qualified to quantify work hardening. All the experimental tests described in Table 1 have thus been numerically simulated and the results correlated with the experimental measurements.

3.1 Model for plasticity

The chosen constitutive model is an elasto-visco-plastic model proposed by Chaboche *et al.* [21]. In this model, the total strain tensor $\boldsymbol{\varepsilon}$ is additively decomposed into the elastic $\boldsymbol{\varepsilon}^{e}$ and plastic $\boldsymbol{\varepsilon}^{p}$ strain tensors. The elastic domain is defined by $f \leq 0$ in the stress space $\boldsymbol{\sigma}$ with:

$$f=J(\sigma-\boldsymbol{X})-R \qquad \text{Eq. 1}$$

where the function J returns the von Mises invariant, R indicates the size of the instantaneous yield condition and $\boldsymbol{X}$ is the back stress tensor. The plastic strain rate tensor $\dot{\boldsymbol{\varepsilon}}^{\boldsymbol{p}}$ is obtained with the flow rule, using the normality assumption:

$$\dot{\boldsymbol{\varepsilon}}^{\boldsymbol{p}} = \dot{\boldsymbol{\lambda}}\frac{\partial \boldsymbol{f}}{\partial \boldsymbol{\sigma}} \qquad \textbf{Eq. 2}$$

where the dot represents the differentiation with respect to time and the plastic multiplier $\dot{\lambda}$ is given by the Norton power law:

$$\dot{\boldsymbol{\lambda}} = \langle\frac{f}{K}\rangle^{\boldsymbol{n}} \qquad \textbf{Eq. 3}$$

To model visco-plasticity. The equivalent plastic strain rate $\dot{p}$ is:

$$\dot{\boldsymbol{p}} = \sqrt{\frac{2}{3}\dot{\boldsymbol{\varepsilon}}^{\boldsymbol{p}}:\dot{\boldsymbol{\varepsilon}}^{\boldsymbol{p}}} \qquad \textbf{Eq. 4}$$

A non-linear isotropic hardening R is defined as the sum of several contributions indexed with "*i*":

$$\boldsymbol{R} = \sum_{\boldsymbol{i}} \boldsymbol{R^i}\ \boldsymbol{with}\ \dot{\boldsymbol{R}}^{\boldsymbol{i}} = \boldsymbol{b_i}(\boldsymbol{Q_i} - \boldsymbol{R^i})\dot{\boldsymbol{p}} \qquad \textbf{Eq. 5}$$

where the b_i and Q_i are material parameters associated to contribution i. Similarly, the back stress $\boldsymbol{X}$ is decomposed as the sum of several contributions, indexed with "k":

$$\boldsymbol{X} = \sum_{\boldsymbol{k}} \boldsymbol{X^k} \qquad \textbf{Eq. 6}$$

with

$$\dot{\boldsymbol{X}}^{\boldsymbol{k}} = \frac{2}{3}\boldsymbol{C_k}\,\dot{\boldsymbol{\varepsilon}}^{\boldsymbol{p}} - \boldsymbol{D_k}\psi(\boldsymbol{X^k})\boldsymbol{X^k}\dot{\boldsymbol{p}} \qquad \textbf{Eq. 7}$$

and where the $\psi(\boldsymbol{X}^k)$ is:

$$\boldsymbol{\psi}(\boldsymbol{X^k}) = \langle\frac{\boldsymbol{D_k}\boldsymbol{J}(\boldsymbol{X^k})-\boldsymbol{\omega_k}\boldsymbol{C_k}}{\boldsymbol{1}-\boldsymbol{\omega_k}}\rangle\ \frac{\boldsymbol{1}}{\boldsymbol{D_k}\boldsymbol{J}(\boldsymbol{X^k})} \qquad \textbf{Eq. 8}$$

where C_k, D_k and ω_k are material parameters associated to each contribution k. Note that the functions $\psi(\boldsymbol{X}^k)$ contain a threshold effect.

3.2 Candidate variables to represent work hardening

Four scalar quantities have been identified in the model presented above able to represent work

hardening and for comparison with the experimental data:

- The von Mises equivalent plastic strain $\varepsilon^p = \sqrt{\frac{2}{3}\boldsymbol{\varepsilon^p}:\boldsymbol{\varepsilon^p}}$, this variable represents an instantaneous level of plasticity, that can increase or decrease;
- The cumulative plastic strain *p:* $p(t) = \int_0^t \dot{p}(s)\, ds$, this variable increases only;
- The von Mises equivalent kinematic hardening *X*=$\sqrt{\frac{3}{2}\boldsymbol{X}:\boldsymbol{X}}$;
- The isotropic hardening *R.*

3.3 Simulation

Each experimental test (see Table 1) has been simulated using the model detailed above with the material parameters for Inconel 718 given in [21]. Note that the fields are homogeneous in the test volume of the samples. Thus, the simulations reduce to solving numerically the chosen constitutive model at a given point of the test volume, given temperature and loading history identified with the results of the experimental campaign. The software Zset (codeveloped by Onera and Ecole des Mines de Paris) has been used for these simulations [31].

3.4 Results

The values obtained for each selected model variable have been correlated with the FWHM of the diffracted X-ray peaks and the KAM parameter computed from the EBSD measurements, and the harness values. All the tests performed in the experimental campaign are uniaxial. It is thus possible to correlate the experimental data and the model variable for a given plastic deformation. Figure 3 presents respectively the FWHM, KAM and the microhardness obtained for each sample as a function of the four values of the variables identified to represent work hardening and resulting from the simulations. These results are presented for the *DA* microstructure and for all types of loading; the

loading is identified with the color of each symbol as defined in Table 1, one symbol corresponding to one test sample.

First, it is remarkable to note that, although the quantities that are evaluated by FWHM, by KAM and by the microhardness are different, the comparison between these quantities for each respective variable leads to very similar results. These figures further show that it is not possible to construct a reverse method using isotropic hardening and cumulative plastic strain. Indeed, for the cyclic tests, the cumulative plastic strain is, logically, more important than in the other samples but the FWHM and KAM remain in the lower range of the graph. For isotropic hardening, the values obtained for the cyclic tests and the compressive tests are very close, whereas the FWHM and the KAM clearly lead to distinct evaluations. The values of the von Mises plastic strain and the equivalent kinematic hardening make it possible to distinguish between all the experimental data.

Both thus seem to be able to quantify a work hardening state. In this study, we chose the von Mises plastic strain because it is equal to the plastic deformation in tensile tests.

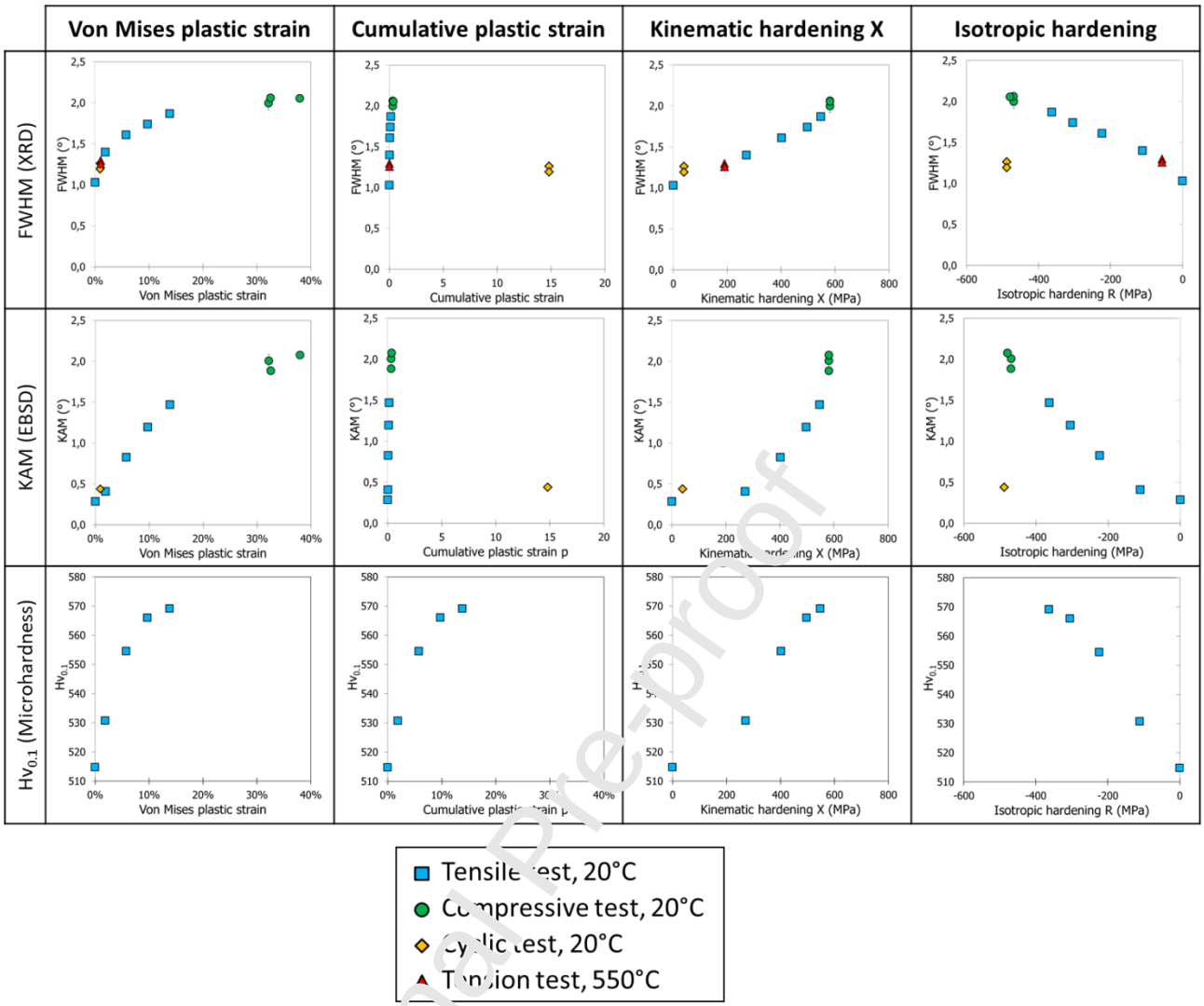

Figure 3. Correlation of the model variables chosen to represent work hardening with the values of the experimental parameters FWHM, KAM and microhardness obtained for each homogeneously loaded specimens for *DA* microstructure.

4 Calibration curves for work hardening

The analyses of the results presented in section 3 lead to the choice of the von Mises equivalent plastic strain to represent the state of work hardening in the samples. It is referred as “the equivalent plastic strain” for simplicity in the rest of this article. This section presents the correlation between the three experimental quantities (microhardness, FWHM and KAM) with this equivalent plastic

strain for all the samples of the experimental campaign: see Figures 4, 5 and 7. Note that each point on these figures corresponds to one mechanical test of Table 1. The results are analyzed and correlation curves are proposed up to 50% of equivalent plastic strains, fitted to the experimental data with a least-square method.

4.1 Microhardness

Figure 4 presents the evolution of the microhardness as a function of the equivalent plastic strain for the tensile tests performed on the three microstructures at 20°C. The figure shows that the microhardness increases with plastic strain. The variability of the microhardness evaluated at different points of the same sample was important; this has been observed for the three microstructures and for all the values of the equivalent plastic strain. The value of the error on the measure is thus important; the error is of the same order as the difference between the microhardness of each microstructure for a given equivalent plastic strain as demonstrated by the error bars in Figure 4.

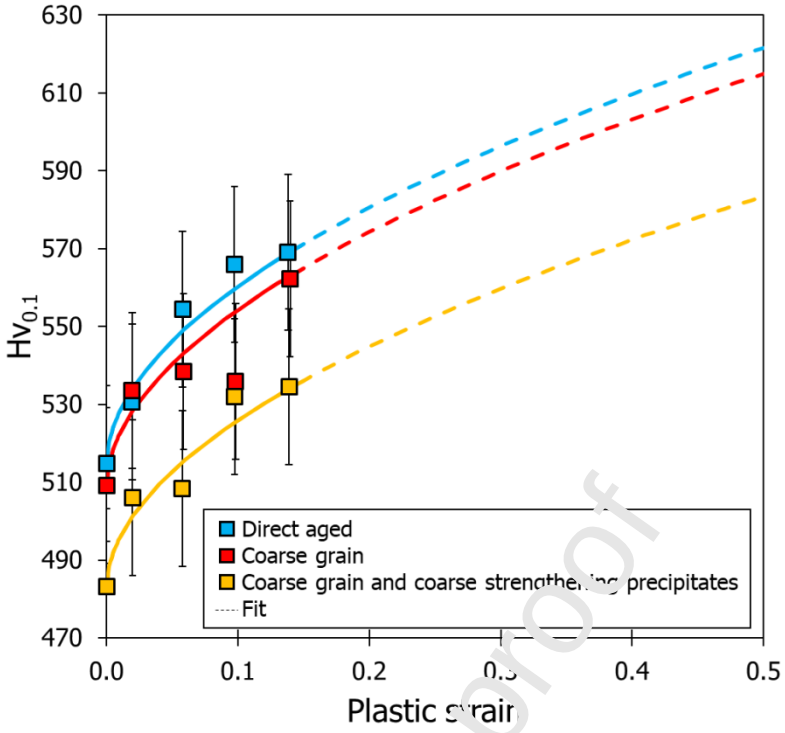

Figure 4. Microhardness as a function of the equivalent plastic strain obtained for the tensile tests at 20°C with the respective calibration curves.

Based on the work of [16], a power law has been chosen to fit the experimental data presented in Figure 4:

$$Hv_{0,1}(\varepsilon_p) = Hv_{0,1}(0)(1 + A{\varepsilon_p}^B) \quad \text{Eq. 9}$$

where $Hv_{0,1}(0)$ is the microhardness in the sample without plastic deformation. Because of the dispersion of the microhardness values, the fit has been performed considering that the three microstructures followed the same power law. With this hypothesis only the $Hv_{0.1}$ value is function of the microstructure. The values of the parameters obtained after the fitting are given in Table 5. In Figure 4, the curves representing the microhardness have been extrapolated up to 50% of equivalent plastic strain (dotted lines) with the function established by the fitting to allow a correlation at high equivalent plastic deformations.

Table 5. Values of the constants obtained for the calibration of the microhardness as a function of the equivalent plastic strain fitted with equation 9 for the three microstructures.

	DA microstructure	Coarse grain microstructure	Coarse grain and coarse strengthening precipitate microstructure
A_{Hv}	0.3		
B_{Hv}	0.53		
$Hv_{0.1}(0)$	514.7	509.2	483.1

It is thus possible to build a correlation curve able to relate the microhardness to the equivalent plastic strain as a function of the microstructure of the material. Due to the dispersion of the measurements obtained during the tests, the use of the calibration curve to deduce an equivalent plastic strain from a measured microhardness is not the most reliable. One of the issues is the size of the indent, and thus the size of the volume analyzed by the method. In the present study, the indent has a rather small size, the analyzed volume being approximately of the same size as the grains for the *coarse* microstructure and the *coarse* microstructure with strengthening precipitates. This fact might explain the irregularity of the measured hardness that, in this case, is more sensitive to the position of the indents (over a grain boundary or in the center of a grain). Also, the microhardness gives a global evaluation on the material state below the indent, sensitive to the hardening state but also to the residual stresses [52]. All the samples tested in this calibration study were free of residual stresses. If residual stresses are present in the part, the use of the microhardness to evaluate the work hardening level might be more problematic. For all these reasons, the microhardness measurements were performed only on the samples submitted to tensile tests at 20°C. Nevertheless, this technique is relatively easy to perform and further investigations on its capacity to evaluate the hardening state of the material might be of interest.

4.2 FWHM from X-ray Diffraction

The correlation between the FWHM obtained by X-ray diffraction and the equivalent plastic strain is presented in Figure 5. The results show that the FWHM increase with the plastic strain and that this is function of the strain rate and the microstructure. The increase of the FWHM is important for low equivalent plastic strains (below 2%) and becomes moderate and linear for higher strains. For the *DA* microstructure and for a strain rate of 10^{-3} s^{-1}, the temperature and loading conditions (tensile, compressive or fatigue tests) have no influence on the measured FWHM value. Indeed, experimental points resulting from these tests induce a common evolution (thin blue line). In contrast, for a given equivalent plastic strain, the FWHM is higher when the strain rate increases (thick blue line). The measured FWHM is sensitive to the strain rates at which the tests have been performed in this study. Further, the two modified microstructures present a similar evolution of the FWHM that is smaller than the FWHM obtained for the *DA* microstructure for a given equivalent plastic strain. Figure 5.b shows that the FWHM also seems to be slightly sensitive to the intragranular microstructure, *i.e.* to the size of the strengthening precipitates.

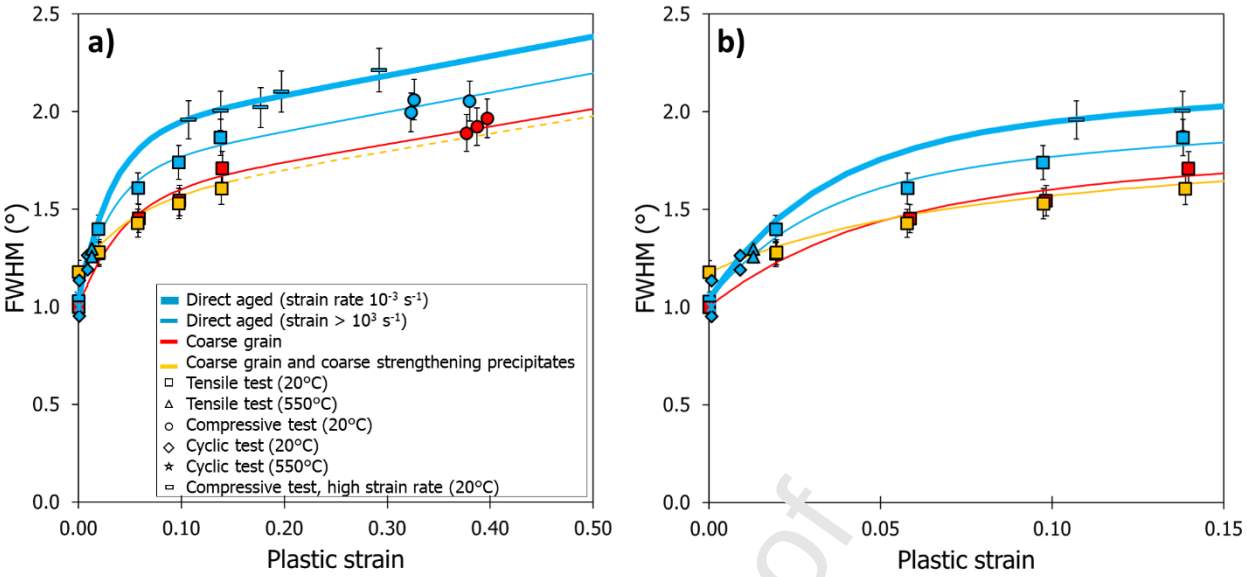

Figure 5. FWHM as a function of the equivalent plastic strain for several loading history, temperature, strain rates and microstructures with the respective calibration curves. b) Close-up of Figure a) for small plastic strains

A function including an exponential increase followed by a straight line has been chosen to fit the data for calibration with the FWHM values [1]:

$$\boldsymbol{FWHM(\varepsilon_p) = A_{FWHM}\left(1 - e^{-B_{FWHM}\varepsilon_p}\right) + C_{FWHM}\,\varepsilon_p + D_{FWHM}} \qquad \textbf{Eq. 10}$$

where A_{FWHM}, B_{FWHM}, C_{FWHM} and D_{FWHM} are parameters that have been evaluated for each microstructure; the results are given in Table 6. Two fits have been established for the *DA* microstructure to take into account the sensitivity to the strain rate. For the microstructure with coarse grains and coarse strengthening precipitates, the straight line for high equivalent plastic strains has been extrapolated parallel to the one corresponding to the *coarse grain* microstructure.

Table 6. Values of the constants obtained for the calibration of the FWHM for the three microstructures as defined by equation 10.

	DA microstructure		Coarse grain micro-structure	Coarse grain and strengthening precip-itate microstructure
	Low strain rates	High strain rates		
A_{FWHM}	0.66	0.85	0.56	0.35
B_{FWHM}	31.12		23.92	20.00
C_{FWHM}	0.99		0.90	
D_{FWHM}	1.04		1.00	1.18

The FWHM value is driven by several factors related to microstructural aspects: grain size, strengthening precipitates size and volume fraction. At a microscopic scale, the size of the coherent domains is preponderant: the smaller they are, the wider the diffraction peak. At a mesoscopic scale, the dislocation arrangements and the several phases impact the FWHM value. Finally at a macroscopic scale, the crystallographic structure and the grain size are the main driving factors [26]. The microstructure has then a major influence on the FWHM values. Therefore a microstructure dependent work hardening calibration is needed for the XRD method as demonstrated in Figure 5.

It should also be noted that X-ray diffraction methods enable to evaluate residual stresses with the shift of the peak, independently of FWHM measurements. This is a real advantage compared to the microhardness measurements.

4.3 KAM from *Electron BackScatter Diffraction*

KAM maps obtained for single tension, single compression and cyclic tests performed at 20°C on the three microstructures are presented in Figure 6 for several levels of equivalent plastic strain. An evolution of the cartography is observed as a function of the plastic deformation. On this scale, there are no significant differences in the distribution of KAM values in the map according to the type of solicitation applied (cyclic test, tensile test and compressive test). On the other hand, the equivalent plastic strain reached in the sample has a major impact on the KAM maps: the higher the strain, the higher the KAM values are. Moreover, the local misorientation tends to increase near grain

boundaries for the three microstructures; it is quite remarkable on *coarse grain* microstructures as it has also been observed in previous studies [14], [30].

Figure 6 demonstrates that, even if the KAM cartography has a size that includes several grains, it is nevertheless possible to extract a global information dependent on the equivalent plastic strain. This is related to the fact that each cartography is different from the other and is rather homogeneous for a given plastic deformation. The average value of the KAM parameter has thus been computed for each cartography and appears to be a meaningful quantity.

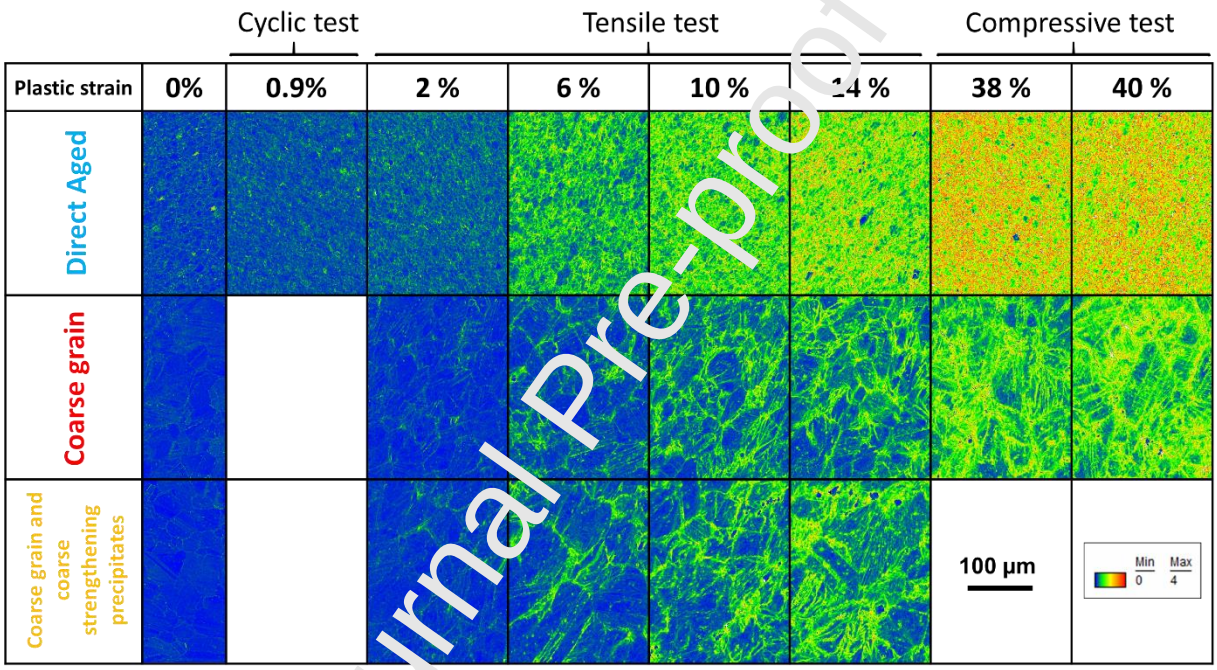

Figure 6. Local misorientation EBSD maps of Direct Aged, *coarse grain* and *coarse grain and coarse strengthening precipitate* microstructures for several equivalent plastic strain levels.

The relationship between the mean KAM parameter and the equivalent plastic strain is presented in Figure 7 for single tension, single compression and cyclic tests performed at 20°C, for the three studied microstructures. As observed previously on the detailed maps of Figure 6, the mean value of the KAM parameter increases as the plastic deformation rises. For the three microstructures, the most significant increase in the mean value of the KAM parameter occurs for a value of the equivalent plastic strain between 0 and 15%. After 15%, the evolution of the KAM parameter is less

pronounced for the Direct Aged microstructure.

The two microstructures featuring coarse grains present the same evolution for the KAM parameter as a function of the equivalent plastic strain, smaller than the KAM values obtained for the *DA* microstructure. Thus, the grain size seems to be a predominant factor in the EBSD calibration. These results are to be compared with the density of grain boundaries, that is higher in the case of the *DA* microstructure with a smaller grain size. Indeed, since the values of the KAM parameter are higher close to grain boundaries, the mean KAM values are necessarily more important for a microstructure with a higher grain boundary density, I.e. a smaller grain size.

The difference in the values of the KAM at 0% of plastic strain could be related to the thermomechanical history of the samples that is different between the *DA* microstructure and *coarse grain* microstructures. Indeed, in the case of *coarse grain* microstructures, an annealing at 1040 °C during 30 minutes has been performed, generating a decrease in the plastic deformation induced during the manufacturing stages performed to produce the reference microstructure (notably during forging).

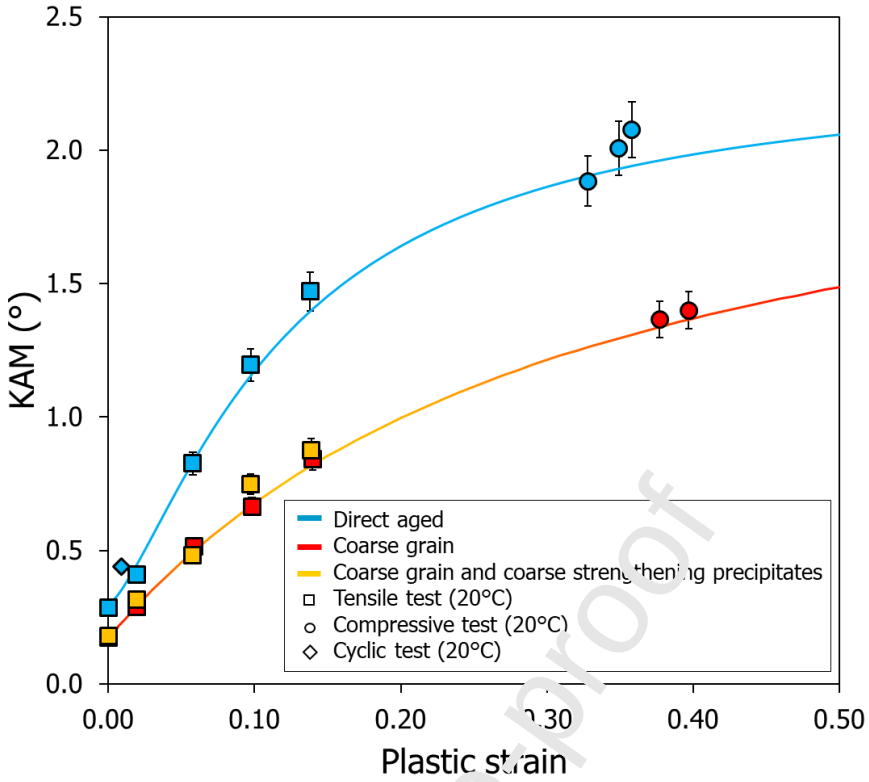

Figure 7. KAM parameter as a function of the equivalent plastic strain for different loading history and microstructures with the respective calibration curves.

The evolution of the KAM parameter versus the equivalent plastic strain has been fitted with the Roadbard function used by [17]:

$$\boldsymbol{KAM(\varepsilon_p) = D_{EBSD} + \frac{(A_{EBSD} - D_{EBSD})}{\left[1+\left(\frac{\varepsilon_p}{C_{EBSD}}\right)^{B_{EBSD}}\right]}} \qquad \textbf{Eq. 11}$$

Where A_{EBSD}, B_{EBSD}, C_{EBSD} and D_{EBSD} are the parameters to be determined with the fitting. A_{EBSD} is the value of the KAM at the origin, for a value of the equivalent plastic strain equal to zero, B_{EBSD} is the initial slope, C_{EBSD} corresponds to the position of the transition region and D_{EBSD} corresponds to the positions of the asymptote for large equivalent plastic deformation [33]. The values of these constants obtained for each microstructure are listed in Table 7. No difference has been made for the fitting of the *coarse grain* microstructure.

Table 7. Values of the constants obtained for the calibration curves as defined by equation 11 with the fitting of the KAM parameter for the three microstructures.

	DA microstructure	Coarse grain microstructure and Coarse grain and strengthening precipitate microstructure
A_{EBSD}	0.30	0.18
B_{EBSD}	1.39	1.03
C_{EBSD}	0.12	0.31
D_{EBSD}	2.30	2.20

The EBSD technique allows the detection of geometrically necessary dislocations that represent around 15 to 30 % of the overall dislocations [29], but are of primary importance in order to understand the plastic deformation and then describe the evolution of the work hardening. As the geometrically necessary dislocations density is mainly sensitive to activities close to the grain boundaries, the KAM value measured by EBSD will be greater for fine microstructures which are characterized with higher grain boundary densities (see the higher KAM levels for the *DA* microstructure in Figure 7). A work hardening calibration depending on the microstructure is therefore of interest to characterize work hardening.

5 Conclusion

The objective of this article is to propose a methodology to define and quantify the level of work hardening locally in a material, taking into account the influence of the type of loading, the temperature, the strain rate and the microstructure. We thus proposed an experimental campaign including a wide range of conditions: in particular several loading histories that enabled to establish the calibration up to an equivalent plastic strain of 50%. Cyclic loadings and high strain rates have also been

considered to determine the sensitivity of the correlation method to these factors. Three microstructures have been tested to evaluate the influence of the size of the grains and strengthening precipitates. The results demonstrate that the measurements performed with the three techniques (microhardness, FWHM of XRD and KAM of EBSD) are sensitive to the microstructure and that this sensitivity depends on the characterization technique.

It may be concluded that the three techniques offer a certain complementarity:

- The microhardness gives a global information on the mechanical state of the analyzed volume. The correlation of the measurements with an equivalent plastic deformation is possible, even if the dispersion of the data is important. The fact that the microhardness also depends on the residual stress can become problematic when evaluating work hardening in a structure.

- The equivalent plastic strain is well correlated with FWHM of XRD and a correlation taking the strain rate into account has been established. Its resolution is compatible with the evaluation of gradients in a complex mechanical part. In addition, since the same measurements can be used to characterize plastic deformation and residual stresses this technic presents a great interest.

- The average KAM parameter of EBSD is well correlated with the equivalent plastic deformation. The advantage of this method resides in the fact that it gives very local information that stays meaningful when averaged.

Simulations have been performed for each experimental test with a pertinent elasto-visco-plastic model. A correlation between the model variables and the experimental parameters (FWHM, KAM and microhardness) enables to choose the equivalent plastic strain as a variable representative of the work hardening state in the material. This methodology has been applied on Inconel 718 but we expect it to remain relevant for any metals. The chosen experimental techniques are classically used on metals with different crystal structures. The constitutive model can be similarly declined on a large

range of metallic materials. By implementing this approach, it is therefore possible, with certain precautions, to use the calibration curves and determine the work hardening state in a mechanical part. The evaluation of the work hardening induced by different manufacturing processes (forging, rolling, shot-peening, ...) could be an interesting application of the proposed methodology.

Acknowledgement

This work was conducted with the help of the French Technological Research Institute for Materials, Metallurgy and Processes (IRT M2P) under the CONDOR project. The authors would like to acknowledge IRT M2P and all the partners of the project led by IRT M2P. Safran is warmly thanked for its precious collaboration in this work.

Data availability

The raw/processed data required to reproduce these findings cannot be shared at this time due to legal or ethical reasons.

References

[1] P. S. Prevey, "The Effect of Cold Work on the Thermal Stability of Residual Compression in Surface Enhanced IN718," St. Louis, Missouri, 2000.

[2] J. T. Cammett, P. S. Prevey, and N. Jayaraman, "The effect of shot peening coverage on residual stress, cold work, and fatigue in a Nickel-Base Superalloy," Paris, 2005.

[3] M. Benedetti, V. Fontanari, C. Santus, and M. Bandini, "Notch fatigue behaviour of shot peened high-strength aluminium alloys: Experiments and predictions using a critical distance method," *International Journal of Fatigue*, vol. 32, no. 10, pp. 1600–1611, Oct. 2010, doi: 10.1016/j.ijfatigue.2010.02.012.

[4] Md. S. Bhuiyan, Y. Mutoh, and A. J. McEvily, "The influence of mechanical surface treatments on fatigue behavior of extruded AZ61 magnesium alloy," *Materials Science and Engineering: A*, vol. 549, pp. 69–75, Jul. 2012, doi: 10.1016/j.msea.2012.04.007.

[5] A. Gariépy, F. Bridier, M. Hoseini, P. Bocher, C. Perron, and M. Lévesque, "Experimental and numerical investigation of material heterogeneity in shot peened aluminium alloy AA2024-T351," *Surface and Coatings Technology*, vol. 219, pp. 15–30, Mar. 2013, doi: 10.1016/j.surfcoat.2012.12.046.

[6] A. T. Vielma, V. Llaneza, and F. J. Belzunce, “Effect of coverage and double peening treatments on the fatigue life of a quenched and tempered structural steel,” *Surface and Coatings Technology*, vol. 249, pp. 75–83, 2014, doi: 10.1016/j.surfcoat.2014.03.051.

[7] B. Gerin, E. Pessard, F. Morel, and C. Verdu, “Influence of surface integrity on the fatigue behaviour of a hot-forged and shot-peened C70 steel component,” *Materials Science and Engineering: A*, vol. 686, pp. 121–133, 2017, doi: 10.1016/j.msea.2017.01.041.

[8] T. Klotz, D. Delbergue, P. Bocher, M. Lévesque, and M. Brochu, “Surface characteristics and fatigue behavior of shot peened Inconel 718,” *International Journal of Fatigue*, vol. 110, pp. 10–21, May 2018, doi: 10.1016/j.ijfatigue.2018.01.005.

[9] D. Kumar, I. Sridhar, W. Wei, and S. Narasimalu, “Effect of Surface Mechanical Treatments on the Microstructure-Property-Performance of Engineering Alloys,” *Materials*, vol. 12, p. 2503, Aug. 2019, doi: 10.3390/ma12162503.

[10] J. Hoffmeister, V. Schulze, R. Hessert, and G. Koenig, “Effects of the surface treatment on the measured diffraction peak width of Inconel 718,” in *ICSP-11*, 2011, pp. 201–206, Accessed: Apr. 11, 2017. [Online]. Available: http://www.shotpeener.com/library/pdf/2011033.pdf.

[11] P. Juijerm and I. Altenberger, “Residual stress relaxation of deep-rolled Al–Mg–Si–Cu alloy during cyclic loading at elevated temperatures,” *Scripta Materialia*, vol. 55, no. 12, pp. 1111–1114, 2006, doi: 10.1016/j.scriptamat.2006.08.047.

[12] K. Dalaei, B. Karlsson, and L.-E. Svensson, “Stability of shot peening induced residual stresses and their influence on fatigue lifetime,” *Materials Science and Engineering: A*, vol. 528, no. 3, pp. 1008–1015, Jan. 2011, doi: 10.1016/j.msea.2010.09.050.

[13] P. S. Prevey, “The measurement of sub-surface residual stress and cold work distributions in nickel base alloys,” in *Residual Stress in Design, Process and Materials Selection*, 1987, pp. 11–19.

[14] M. Kamaya, A. J. Wilkinson, and J. M. Titchmarsh, “Measurement of plastic strain of polycrystalline material by electron backscatter diffraction,” *Nuclear Engineering and Design*, vol. 235, pp. 713–725, 2004.

[15] B. J. Foss, S. Gray, M. C. Hardy, S. Stekovic, D. S. McPhail, and B. A. Shollock, “Analysis of shot-peening and residual stress relaxation in the nickel-based superalloy RR1000,” *Acta Materiala*, vol. 61, pp. 2548–2559, 2013.

[16] K. A. Soady, B. G. Mellor, G. D. West, G. Harrison, A. Morris, and P. A. S. Reed, “Evaluating surface deformation and near surface strain hardening resulting from shot peening a tempered martensitic steel and application to low cycle fatigue,” *International Journal of Fatigue*, vol. 54, pp. 106–117, Sep. 2013, doi: 10.1016/j.ijfatigue.2013.03.019.

[17] D. N. Githinji, S. M. Northover, P. J. Bouchard, and M. A. Rist, “An EBSD Study of the Deformation of Service-Aged 316 Austenitic Steel,” *Metall and Mat Trans A*, vol. 44, no. 9, pp. 4150–4167, Sep. 2013, doi: 10.1007/s11661-013-1787-7.

[18] R. R. Shen, V. Ström, and P. Efsing, “Spatial correlation between local misorientations and nanoindentation hardness in nickel-base alloy 690,” *Materials Science and Engineering: A*, vol. 674, pp. 171–177, Sep. 2016, doi: 10.1016/j.msea.2016.07.123.

[19] Y. Lv, L. Lei, and L. Sun, “Effect of shot peening on the fatigue resistance of laser surface melted 20CrMnTi steel gear,” *Materials Science and Engineering: A*, vol. 629, pp. 8–15, 2015, doi: 10.1016/j.msea.2015.01.074.

[20] Y. Lv, L. Lei, and L. Sun, “Influence of different combined severe shot peening and laser surface melting treatments on the fatigue performance of 20CrMnTi steel gear,” *Materials Science and Engineering: A*, vol. 658, pp. 77–85, Mar. 2016, doi: 10.1016/j.msea.2016.01.050.

[21] J.-L. Chaboche, P. Kanouté, and F. Azzouz, “Cyclic inelastic constitutive equations and their impact on the fatigue life predictions,” *International Journal of Plasticity*, vol. 35, pp. 44–66, Aug. 2012, doi: 10.1016/j.ijplas.2012.01.010.

[22] T. Heuzé, X. Guo, and R. Othman, "Very High Strain Rate Range," in *The Kolsky-Hopkinson Bar Machine*, Springer International Publishing, 2018, pp. 249–272.
[23] D. Tabor, "The physical meaning of indentation and scratch hardness," *British Journal of Applied Physics*, vol. 7, no. 5, p. 159, 1956, doi: 10.1088/0508-3443/7/5/301.
[24] J. R. Cahoon, W. H. Broughton, and A. R. Kutzak, "The determination of yield strength from hardness measurements," *Metallurgical Transactions*, vol. 2, no. 7, pp. 1979–1983, 1971, doi: 10.1007/BF02913433.
[25] G. Srikant, N. Chollacoop, and U. Ramamurty, "Plastic strain distribution underneath a Vickers Indenter: Role of yield strength and work hardening exponent," *Acta Materialia*, vol. 54, no. 19, pp. 5171–5178, Nov. 2006, doi: 10.1016/j.actamat.2006.06.032.
[26] S. for E. Mechanics (U.S.), *Handbook of Measurement of Residual Stresses*. Fairmont Press, 1996.
[27] S. I. Wright, M. M. Nowell, and D. P. Field, "A Review of Strain Analysis Using Electron Backscatter Diffraction," *Microscopy and Microanalysis*, vol. 17, no. 3, pp. 316–329, Jun. 2011, doi: 10.1017/S1431927611000055.
[28] A. Sáez-Maderuelo, L. Castro, and G. de Diego, "Plastic strain characterization in austenitic stainless steels and nickel alloys by electron backscatter diffraction," *Journal of Nuclear Materials*, vol. 416, no. 1–2, pp. 75–79, Sep. 2011, doi: 10.1016/j.jnucmat.2010.11.092.
[29] H. Gao and Y. Huang, "Geometrically necessary dislocation and size-dependent plasticity," *Scripta Materialia*, vol. 48, no. 2, pp. 113–118, Jan. 2003, doi: 10.1016/S1359-6462(02)00329-9.
[30] D. P. Field, C. C. Merriman, N. Allain-Bonasso, and F. Wagner, "Quantification of dislocation structure heterogeneity in deformed polycrystals by EBSD," *Modelling and Simulation in Materials Science and Engineering*, vol. 20, no. 2, p. 024007, 2012, doi: 10.1088/0965-0393/20/2/024007.
[31] J. Besson, G. Cailletaud, J.-L. Chaboche, and S. Forest, *Non-Linear Mechanics of Materials*. Springer Netherlands, 2010.
[32] Y. G. Li, P. Kanoute, and M. François, "Characterization of Residual Stresses and Accumulated Plastic Strain Induced by Shot Peening through Simulation of Instrumented Indentation," *Advanced Materials Research*, vol. 996, pp. 367–372, 2014, doi: 10.4028/www.scientific.net/AMR.996.367.
[33] P. G. Gottschalk and J. R. Dunn, "The five-parameter logistic: A characterization and comparison with the four-parameter logistic," *Analytical Biochemistry*, vol. 343, no. 1, pp. 54–65, 2005, doi: 10.1016/j.ab.2005.04.035.

Highlights

- The measurements performed are sensitive to the microstructure
- Correlate the level of equivalent plastic deformation with EBSD measurements
- Correlate the level of equivalent plastic deformation with XRD measurements
- Sensitivity to the microstructure is dependent on the characterization technique
- The characterization methods are complementary to determine work hardening